

Near-field and far-field analysis of an azimuthally polarized slow Bloch mode microlaser

Thanh-Phong Vo¹, Adel Rahmani², Ali Belarouci¹, Christian Seassal¹, Dusan Nedeljkovic³ and Ségolène Callard^{1,*}

¹Université de Lyon, Institut des nanotechnologies de Lyon INL-UMR 5270, CNRS, Ecole Centrale de Lyon, Avenue Guy de Collongue, F-69134 Cedex, France

²Department of Mathematical Science, University of Technology, Sydney, NSW 2007 Australia

³Loyalite s.a.s. 18 rue Alain Savary, 25000 Besançon, France

*segolene.callard@ec-lyon.fr

Abstract: We report on the near- and far-field investigation of the slow Bloch modes associated with the Γ point of the Brillouin zone, for a honeycomb lattice photonic crystal, using near-field scanning optical microscopy (NSOM) and infra-red CCD camera. The array of doughnut-shaped monopolar mode (mode M) inside each unit cell, predicted previously by numerical simulation, is experimentally observed in the near-field by means of a metal-coated NSOM tip. In far-field, we detect the azimuthal polarization of the doughnut laser beam due to destructive and constructive interference of the mode radiating from the surface (mode TEM_{01*}). A divergence of 2° for the laser beam and a mode size of (12.8 ± 1) μm for the slow Bloch mode at the surface of the crystal are also estimated.

©2010 Optical Society of America

OCIS codes: (180.4243) Near-field microscopy; (350.4238) Nanophotonics and photonic crystals; (250.7270) Vertical emitting lasers.

References and links

1. K. Sakoda, *Optical Properties of Photonic Crystals*, (Springer- Verlag, Berlin, Heidelberg, 2001).
2. J. D. Joannopoulos, S. G. Johnson, J. N. Winn, and R. D. Meade, *Photonic Crystals: molding the flow of the light*, (Princeton University Press, 2008).
3. M. Notomi, "Manipulating light with strongly modulated photonic crystals," *Rep. Prog. Phys.* **73**(9), 096501 (2010).
4. P. Viktorovitch, B. B. Bakir, S. Boutami, J. L. Leclercq, X. Letartre, P. R. Romeo, C. Seassal, M. Zussy, L. Di Cioccio, and J. M. Fedeli, "3-D harnessing of light with 2.5 D photonic Crystals," *Laser Photon. Rev.* **4**(3), 401–413 (2010).
5. F. Raineri, C. Cojocar, R. Raj, P. Monnier, A. Levenson, C. Seassal, X. Letartre, and P. Viktorovitch, "Tuning a two-dimensional photonic crystal resonance via optical carrier injection," *Opt. Lett.* **30**(1), 64–66 (2005).
6. B. B. Bakir, Ch. X. Letartre, P. Viktorovitch, M. Zussy, L. Di Cioccio, and J. M. Fedeli, "Surface-emitting microlaser combining two-dimensional photonic crystal membrane and vertical Bragg mirror," *Appl. Phys. Lett.* **88**, 8 (2006).
7. K. Sakai, E. Miyai, T. Sakaguchi, D. Ohnishi, T. Okano, and S. Noda, "Lasing band-edge identification for a surface-emitting photonic crystal laser," *IEEE J. Sel. Areas Comm.* **23**(7), 1335–1340 (2005).
8. K. Sakai, and S. Noda, "Optical trapping of metal particles in doughnut-shaped beam emitted by photonic-crystal laser," *Electron. Lett.* **43**(2), 107 (2007).
9. E. Miyai, K. Sakai, T. Okano, W. Kunishi, D. Ohnishi, and S. Noda, "Photonics: lasers producing tailored beams," *Nature* **441**(7096), 946 (2006).
10. S.-H. Kwon, and Y.-H. Lee, "High Index-Contrast 2D Photonic Band-Edge Laser," *IEICE Trans. Electron.* **87**, 308 (2004).
11. J.-M. Gérard, and B. Gayral, "Strong Purcell effect for InAs quantum boxes in three-dimensional solid-state microcavities," *J. Lightwave Technol.* **17**(11), 2089–2095 (1999).
12. X. Letartre, J. Mouette, J. L. Leclercq, P. R. Romeo, C. Seassal, and P. Viktorovitch, "Switching devices with spatial and spectral resolution combining photonic crystal and MOEMS structures," *J. Lightwave Technol.* **21**(7), 1691–1699 (2003).
13. L. Ferrier, P. Rojo-Romeo, E. Drouard, X. Letartre, and P. Viktorovitch, "Slow Bloch mode confinement in 2D photonic crystals for surface operating devices," *Opt. Express* **16**(5), 3136–3145 (2008).
14. F. Bordas, M. J. Steel, C. Seassal, and A. Rahmani, "Confinement of band-edge modes in a photonic crystal slab," *Opt. Express* **15**(17), 10890–10902 (2007).
15. A. Belarouci, T. Benyattou, X. Letartre, and P. Viktorovitch, "3D light harnessing based on coupling engineering between 1D-2D Photonic Crystal membranes and metallic nano-antenna," *Opt. Express* **18**(S3), A381–A394 (2010).
16. N. Louvion, D. Gérard, J. Mouette, F. de Fornel, C. Seassal, X. Letartre, A. Rahmani, and S. Callard, "Local observation and spectroscopy of optical modes in an active photonic-crystal microcavity," *Phys. Rev. Lett.* **94**(11), 113907 (2005).
17. G. Le Gac, A. Rahmani, C. Seassal, E. Picard, E. Hadji, and S. Callard, "Tuning of an active photonic crystal cavity by an hybrid silica/silicon near-field probe," *Opt. Express* **17**(24), 21672–21679 (2009).

18. C. Monat, C. Seassal, X. Letartre, P. Regreny, P. Rojo Romeo, P. Viktorovitch, M. Le Vassor d'Yerville, D. Cassagne, J. P. Albert, E. Jalaguier, S. Pocas, and B. Aspar, "InP-based two-dimensional photonic crystal on silicon: InP-plane Bloch mode laser," *Appl. Phys. Lett.* **81**(27), 5102 (2002).
19. C. Monat, C. Seassal, X. Letartre, P. Regreny, M. Gendry, P. R. Romeo, P. Viktorovitch, M. Le Vassor d'Yerville, D. Cassagne, J. P. Albert, E. Jalaguier, S. Pocas, and B. Aspar, "Two-dimensional hexagonal-shaped microcavities formed in a two-dimensional photonic crystal on an InP membrane," *J. Appl. Phys.* **93**(1), 23 (2003).
20. R. Stöckle, C. Fokas, V. Deckert, R. Zenobi, B. Sick, B. Hecht, and U. P. Wild, "High-quality near-field optical probes by tube etching," *Appl. Phys. Lett.* **75**(2), 160 (1999).
21. R. Bachelot, C. Ecoffet, D. Deloëil, P. Royer, and D. J. Lounnot, "Integration of micrometer-sized polymer elements at the end of optical fibers by free-radical photopolymerization," *Appl. Opt.* **40**(32), 5860–5871 (2001).
22. G. Machavariani, Y. Lumer, I. Moshe, and S. Jackel, "Transforming the (0,1)* LG mode with radial polarization to a nearly Gaussian beam by use of a spiral phase element and spatial filter," *Proc. SPIE* **6346**, 63461W (2006).
23. M. Mivelle, I. A. Ibrahim, F. Baida, G. W. Burr, D. Nedeljkovic, D. Charrat, J.-Y. Rauch, R. Salut, and T. Grosjean, "Bowtie nano-aperture as interface between near-fields and a single-mode fiber," *Opt. Express* **18**(15), 15964–15974 (2010).

1. Introduction

2D-Photonic crystal (PC) structures have enabled the fabrication of a wide variety of nanophotonic components [1,2]. In perfect PCs, the exploitation of the enhanced local density of states at critical points of the band diagram has attracted considerable attention [3–6]. Near these points, low curvature flat bands give rise to delocalized and stationary optical slow Bloch modes (SBMs). These properties make them good candidates to enhance Purcell or various non-linear effects [5] or to design low-threshold lasers [6]. Among these modes, SBMs emitting in the vertical direction, i.e. located at the Γ -point of the Brillouin zone are particularly interesting for integrating 2D PC architectures with free space optics. In particular, SBMs have proved to be suitable for achieving strong vertical emission with peculiar polarization properties [7–10]. One of the important features of these modes is their global lateral expansion inside the PC. Theoretically, the expansion, i.e. the mode surface (S) is proportional to the band curvature (which is intrinsic to the 2D-PC design) and to τ , the lifetime of the mode in the structure [11,12]. The lifetime is linked to the coupling time τ_c between the SBM and radiating modes and τ_{loss} , which is related to other losses (associated to PC defects, lateral escape of photons and modal mismatch). In the case of an active structure, like a micro-laser, the mode expansion can also be governed by other mechanisms involving carrier-induced refractive-index change [5]. Indeed, having a direct access to the mode surface is an important way to gain a better understanding of the mode confinement mechanisms. While introducing defects in the PC can be a very effective way to confine SBMs to a very small size [13,14], some applications, which require a good coupling between a SBM and free-space radiation modes [15], require a spatially broader SBM and it is therefore important to investigate how SBM behave in a defect-free PC structure.

Conventional optical characterization techniques, such as micro-photoluminescence, give valuable information on the far-field pattern of the mode. However, they fail to reveal the actual size of the mode as only radiating light is collected. On the other hand, near-field optical microscopy enables us to visualize the evanescent component of the mode with a spatial resolution below the diffraction limit [16]. Consequently, in accordance with the convention of near-field optics, the term near-field will be reserved here to processes that involves evanescent waves which currently occur in within less of a half wavelength of the sample. In this paper, we present a far-field and a near-field study of a 2D-PC Γ -point SBM laser mode. We show that the far-field and the near-field image of the mode at the 2D-PC surface are different. Far-field results show the direct production of azimuthally polarized doughnut mode. As opposed, near-field results yield a better insight in the real mode structure inside the PC slab in agreement with theoretical prediction. An accurate estimate of the mode size can be inferred from NSOM measurements. We also show that for a Γ -point mode, the nature of the NSOM probe is a crucial issue in obtaining the real mode profile. Here, we focused on the fundamental mode of a 2D-PC honeycomb lattice of air holes in an InP membrane incorporating quantum wells. In the first part, the theoretical spatial and spectral properties of the mode are described. Secondly, a far-field polarization analysis of the SBM mode is presented. We then present NSOM experimental results obtained with two types of probe: classical bare silica tip and metal-coated aperture tips.

2. Structure design and simulation

The PC design consists of an honeycomb lattice of cylindrical air holes (with a lattice parameter $A = 730$ nm and a 245 nm hole diameter) patterned in a 240 nm thick InP slab bonded on top of a SiO_2 substrate. The PC structure is designed to support a low curvature band-edge mode at the

Γ point of the first- Brillouin zone [5,6]. The optical response of the structure was modeled using 3D finite-difference time domain method (3D-FDTD) with perfectly matched layers boundary conditions. The size of the PC structure is about $20 \times 20 \mu\text{m}^2$ and consists of the PC slab on a $2 \mu\text{m}$ SiO_2 substrate. Computational meshes were 30 nm for x , y , and z . The monopolar mode is excited with a dipole placed near the center of the structure. Figure 1 presents the mode intensity pattern, computed at the surface of the InP slab, for the band edge mode of lowest energy, labeled M-mode for monopolar mode.

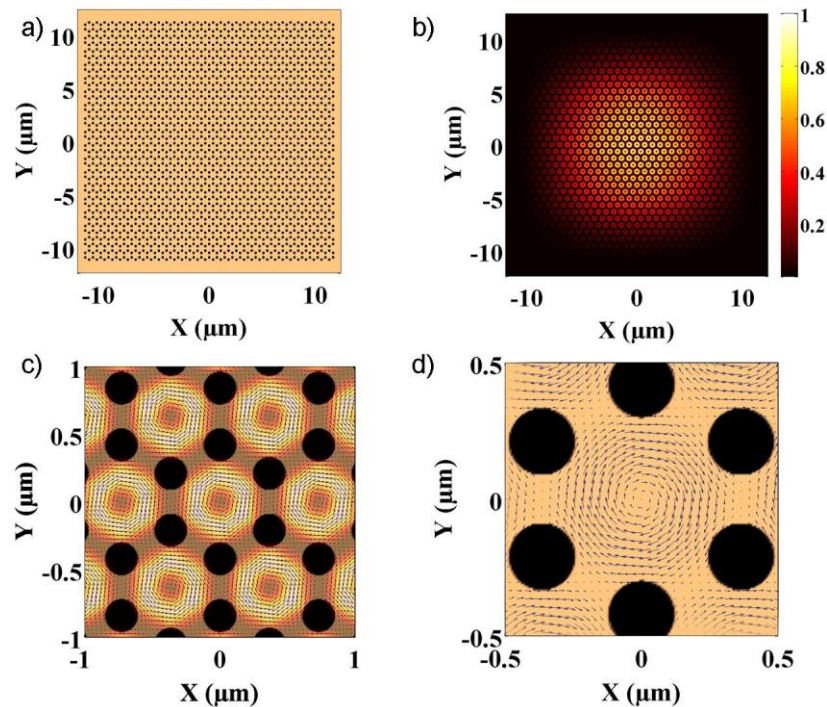


Fig. 1. 3D-FDTD simulation of the monopolar mode at the surface of a 2D-PC slab honeycomb structure. a) Overview of the PC structure. b) Normalized field intensity ($E_x^2 + E_y^2$) at the surface of the PC at 1602 nm . c) Zoom over the central part of the PC showing intensity map with the air holes in black, d) Electric field pattern illustrating the azimuthally polarized field in each unit cell.

The simulation shows that the mode surface is limited by the edge of the PC-structure. The mode intensity is maximum in the centre of the PC and its global envelop is gaussian. Moreover, simulations indicate that the intensity is distributed in each honeycomb lattice unit cell as a doughnut of about 260 nm of outer radius and 90 nm of inner radius. The polarization of the electric field is indeed azimuthally polarized in each unit cell: the zero of the intensity of the field at the centre of each hexagon is due to the phase singularity.

3. Experiments

The InP slab is single mode near $1.55 \mu\text{m}$ and includes at its center four InAsP quantum wells (QW), separated by InP barrier layers. The photoluminescence from the QWs occurs between 1350 nm and 1650 nm . This heterostructure is wafer-bonded onto the fused silica host substrate [17]. Compared to silicon substrates, this design enables front side and back side photo-excitation of the quantum wells. The PC is prepared by drilling a honeycomb lattice of air holes in the slab using e-beam lithography followed by reactive ion etching [18,19]. The NSOM experimental set up is presented in Fig. 2. It uses a stand alone commercial head (NT-MDT SMENA), positioned at the top of an inverted microscope. Two different kinds of probes were used: home-made bare silica tips [20] and polymer metallized tips [21] with aperture of 100 nm . Both probes were made out of single mode optical fiber at $1.55 \mu\text{m}$ with a core diameter of $9 \mu\text{m}$.

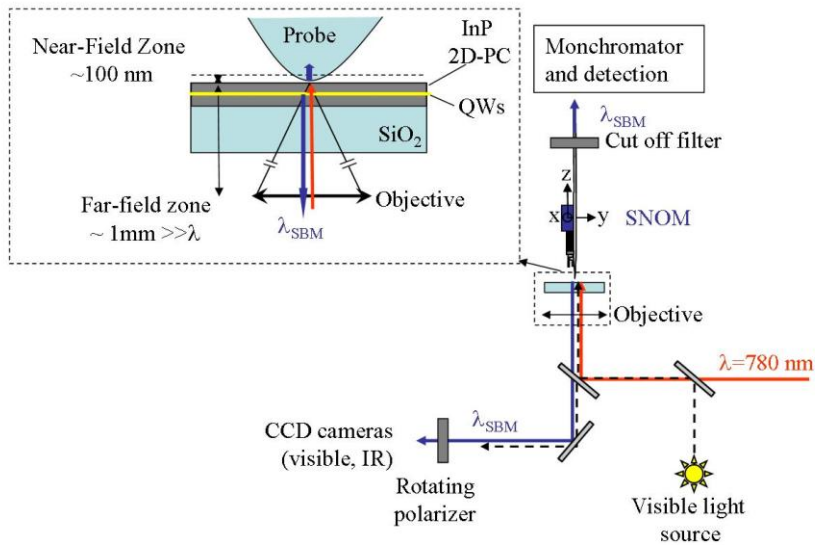


Fig. 2. Experimental set-up: near-field and far-field analysis are implemented.

The NSOM is working in collection mode: the tip collects the photoluminescence (PL) in near-field at the surface of the sample. The PC structures are optically pumped at 780 nm with a pulsed laser diode (with a 10% duty cycle) and modulated at 2 kHz. In this set up the sample is pumped from the back side. The collimated laser beam is focused on the 2D-PC through the silica substrate with a corrected objective (NA = 0.75). The excitation spot focused on the surface has a Gaussian profile and a surface area less than $10\mu\text{m}$ by $10\mu\text{m}$. Its position in the 2D-PC can be controlled accurately with the inverted microscope. The photoluminescence signal is collected in the near-field by the probe and sent to a monochromator (1 nm resolution). A long pass filter is used to eliminate completely the pump light (cutoff wavelength at 1100 nm). The signal is detected with a thermo-electrically cooled InGaAs photodetector. The structure can be investigated over the spectral range between 1350 and 1650 nm. A lock-in amplifier is used to demodulate the signal and enhance the signal to noise ratio. For topography imaging, the fiber is attached to a piezoelectric tuning fork setup which allows a shear-force feedback loop to regulate the distance between tip and sample surface (typically between 5 and 15 nm). In this configuration, topographic and photoluminescence images are recorded simultaneously. Besides, the inverted microscope presents several output allowing the sample observation in far-field in the visible range (silicon CCD camera) and in the IR range (Xeva-076, Xenics).

4. Results and discussion

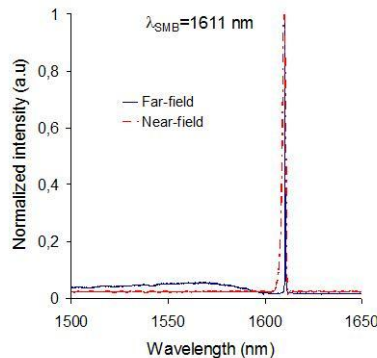


Fig. 3. Far-field and near-field spectra of honeycomb lattice normalized to the maximum intensity. Mode M at $\lambda_{\text{SBM}} = 1611$ nm matching well in two types of measurement.

Figure 3 shows the photoluminescence spectra of the structure recorded in the far-field and in the near-field and measured at room temperature. A strong and sharp peak corresponding to

laser emission was observed at 1611 nm. The peak wavelength is in good agreement with the simulation value found for the monopolar mode (1602 nm). To confirm this assumption, far-field and near-field investigations were conducted to characterize the shape and polarization of the radiated beam and the spatial distribution of the mode inside the structure.

For the far-field study, the inverted microscope was used to form the image of the mode through the NA = 0.75 objective. The image is obtained in far-field (as the objective only collects radiating waves) but it does not constitute a radiation pattern as it corresponds to the spatial distribution of the mode intensity at the surface of the structure. The results are displayed in Fig. 4. The first one (Fig. 4a) is the image recorded without polarizer: it clearly shows a doughnut-shaped mode. This shape is very different to what simulations predict for the mode profile (Fig. 1.) at the surface of structure. However, the doughnut shape can be inferred from the fact that these images are recorded in the far-field where processes of destructive and constructive interferences take place and explain the fading of field in the center of the beam [7].

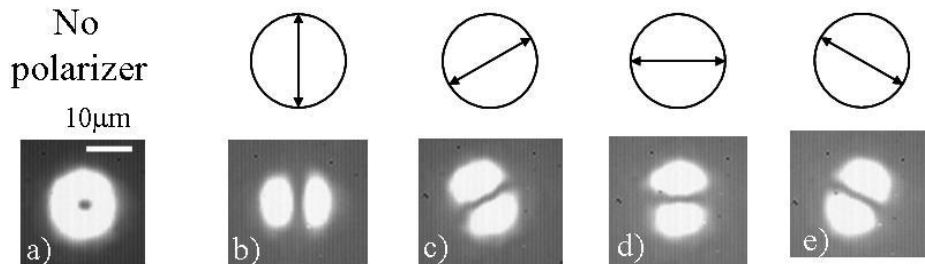


Fig. 4. Image of the mode at the surface of the PC in the far-field zone (the image is collected through a microscope objective with an NA of 0.75). a) Image of the mode without polarizer, b)-e) images with a polarizer oriented respectively at 0°, 60°, 90°, and 120°.

The beam patterns recorded through a polarizer are also shown in Fig. 4. Through the polarizer, the doughnut is transformed into two lobes symmetrically located on either side of the polarizer axis. These results indicate explicitly that the emitted beam is a TEM_{01*} mode with an azimuthal polarization [7–9]. This mode can also be expressed as the coherent superposition of two Hermite-Gauss (HG) beams which have two lobes and no radial symmetry (HG_{10} with x polarization and HG_{01} with y polarization) [22]. The polarizer effect is to select one of the HG modes parallel to its orientation. This demonstrates the direct and simple generation of pure azimuthal doughnut laser beam with a 2D-PC honeycomb lattice.

Near-field inspection of the mode allows a deeper understanding of the mode expansion inside the PC. Two measurements have been performed in the near-field. In the first place, a simple bare silica tip was used to collect the mode intensity at the surface of the 2D-PC. Figure 5c. shows an image recorded with a silicon CCD camera that displayed the contour of the whole PC as well as the position and the size of the excitation spot ($\sim 10\mu\text{m}$ diameter). Figures 5a and 5b present respectively a topographic shear-force image of the structure and the optical image recorded at the wavelength of mode M (1611 nm). Unexpectedly, the near-field image of the mode reveals also a global doughnut shape. Unlike the simulation, this image displayed with the bare silica tip shows that the intensity is minimum at the center of the excitation spot where it should be maximum. Moreover, compared to the far-field image (Fig. 4a), the near-field image shows additional features: the intensity map exhibits a periodic modulation which wavelength fits well the Bloch mode period of the M mode (~ 730 nm). These sub wavelength features confirm that the collection of light takes place in the near-field where the evanescent field is more significant. The presence of the global doughnut shape in near-field can be explained by the fact that the bare silica tip, besides converting evanescent light at the surface to propagating light, is also able to collect a large amount of radiating light through its bare sides. At the Γ point, M-mode emits strongly in the vertical direction to form the doughnut pattern recorded in far-field. At the center of the doughnut of Fig. 5b, where no radiating light is observed due to destructive interference, the optical intensity associated to the evanescent light is estimated to be thirty times weaker than in the ring (Fig. 5d). In order to minimize the contribution of the vertical radiation, one can use a metallized tip with an aperture.

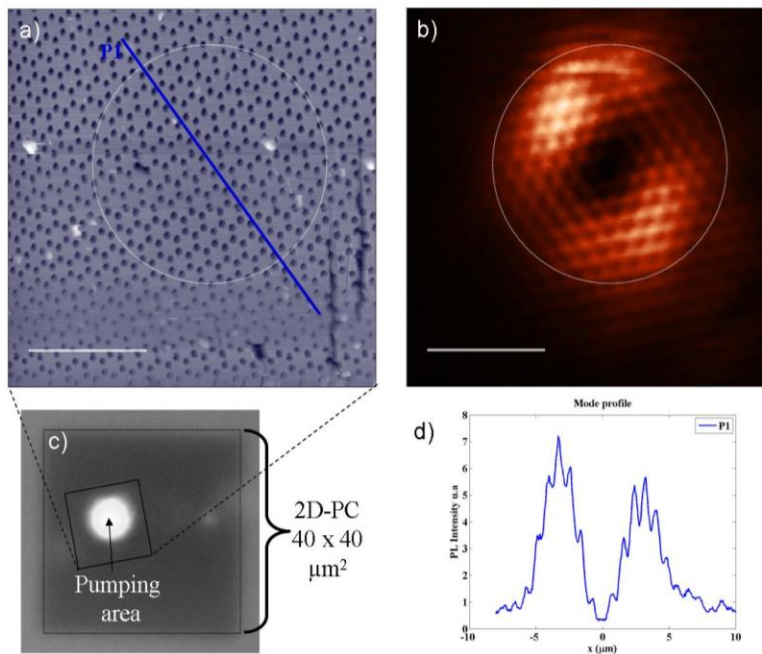


Fig. 5. a) Topography in shear-force mode b) Near-field distribution of intensity of mode-M recorded with a bare silica tip at 1611 nm, the scaling bar is 5 μm , c) CCD image in the visible range of the excitation spot (780 nm) on the structure, the width of the gaussian beam is about 9.5 μm , d) Mode section recorded along the line P1 (corresponding to ΓK direction in the reciprocal space)

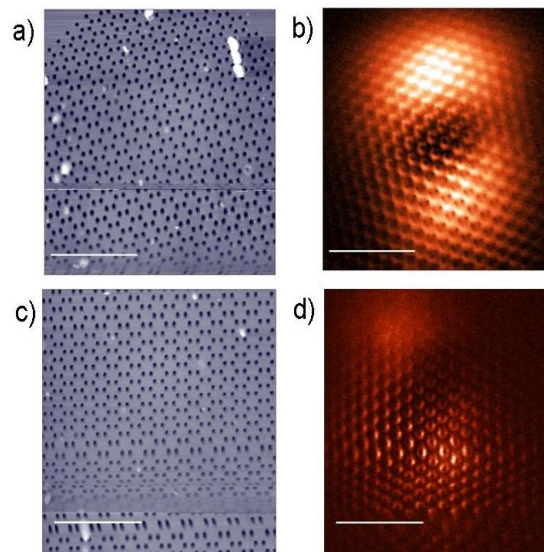


Fig. 6. a) Topography in shear-force mode with metallized tip N°1 b) Near-field distribution of intensity of mode-M recorded with tip N°1 at 1611 nm, the scaling bar is 5 μm , c) Topography with tip N°2, d) Near-field distribution of intensity of mode-M recorded with tip N°2 at 1611 nm, the scaling bar is 5 μm

The topographic and near-field images recorded with two different Al-coated tips are shown in Fig. 6. In the Figs. 6a-6b with tip N°1, the large doughnut still appears. However, new features are also visible in the centre where the radiating field vanishes: in each unit cell of the PC, small doughnuts are clearly visible. In the Figs. 6c-6d with tip N°2, the large doughnut almost disappears to the benefit of a triangular array of small doughnuts which is a clear signature of the monopolar mode as presented in Fig. 1. Indeed, by quantitative measurement, the new contrast of optical intensity between the ring of the large doughnut and its centre is approximately thirteen fold for tip N°1 and fivefold for tip N°2. The difference between the two intensity mapping of Figs. 6b and 6d is probably due to two different aperture sizes of the metallized tips. We assumed that the aperture of tip N°1 is larger than tip N°2 because the

#136880 - \$15.00 USD Received 19 Oct 2010; revised 25 Nov 2010; accepted 1 Dec 2010; published 7 Dec 2010
(C) 2010 OSA 20 December 2010 / Vol. 18, No. 26 / OPTICS EXPRESS 26884

amount of signal collected is higher: it also explained why the resolution of tip N°2 is better. It also confirms that unlike the bare silica tip, the metallized tip succeeds to reveal the fine structure of the SBM. Figure 7 shows that a small doughnut is indeed present in each unit cell of the honeycomb lattice. The dimensions of these doughnuts are 310 nm for the outer radius and 70 nm for the inner radius which is consistent with the theoretical predictions of Fig. 1.

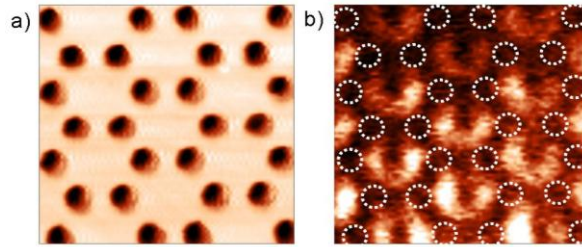


Fig. 7. Detail of the M-mode, a) Topographic image b) Optical near-field image at 1611 nm ($2.5\mu\text{m} \times 2.5\mu\text{m}$), circles indicate holes positions of the 2D-PC. In one unit cell, the outer radius of the doughnut is 310 nm and the inner radius 70 nm ($\lambda/10$).

From near-field images, mode expansion inside the PC can also be inferred. Figure 8a presents the mode expansion recorded under the same excitation conditions as Fig. 6. Though the tip is still collecting an amount of radiating light which accounts for the slight non-uniformity of the mode, it clearly shows that the mode reaches a maximum at the centre and decreases monotonically, in agreement with the predicted, theoretical mode profile (Fig. 1b).

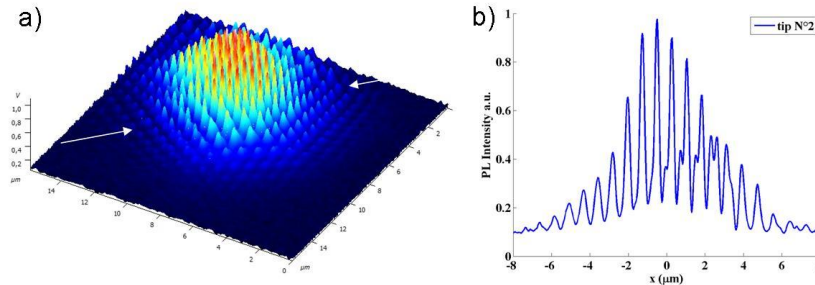


Fig. 8. a) Near-field intensity distribution of mode-M collected with tip N°2 at 1611 nm b) Mode section recorded along the direction of the white arrows of a), .

Cross section recorded along the symmetry axis of the honeycomb lattice (Fig. 8b) yield an estimation of the size of the mode at the surface of the PC: considering the decay of the mode at $1/e^2$, the width of the mode is $(12.8 \pm 1)\mu\text{m}$ which is of the same order of magnitude as the excitation spot. Taking this as the diameter of the beam waist, a divergence of 2° is expected for this beam. The correlation between the excitation spot size and the mode surface tends to confirm the modification of refractive-index induced by the pump. The SBM mode confinement is attributed to the optical well created by the step-index existing between the pumped area and the unpumped area [5]. Experiments with variable pumping area are under progress to study the relationship between the pump size and the mode size.

5. Conclusion

We successfully investigated the distribution of slow Bloch monopolar mode at Γ -point on perfect honeycomb structure both in far-field and near-field. The radiating mode M to the far-field formed a doughnut shape due to destructive and constructive interference. For near-field study by NSOM in collection mode, the array of doughnut patterns repeated by unit cell is obtained. This result enables the unambiguous identification of the monopolar mode with the 3D-FDTD simulations. In addition, the simple and direct generation of pure azimuthally doughnut laser beam with a 2D-PC honeycomb lattice was demonstrated. This opens the way to other perspective for the development of such micro-lasers, as the total field symmetry of azimuthally polarized mode makes it suitable for applications as optical trapping [8] or high numerical aperture focusing. The importance of the tip selection for studying III-V photonic

crystal structures was also demonstrated. With vertical emitting structures bare silica tip is not adapted for near-field mode inspection. Conversely, metallized tip is able to reveal the near-field patterns of the optical modes. However, the collected intensity is much weaker due to the nanoaperture. The ideal tip should be designed to optimize the coupling between the mode and the tip. Functionalized tips with nano-antenna could meet this requirement [23]. Besides, as nano-antenna response is polarization dependent, it should yield local information on the polarization of the mode at the surface.

Acknowledgement

We thank Philippe Regreny for growing the epitaxial structures. The wafer bonding technology was supplied by CEA-LETI. This work was supported by the Agence nationale de la Recherche (Program NANOEC" N ANR07 NANS-036) and by an award under the Merit Allocation Scheme on the National Computational Infrastructure at the Australian National University.